Real-time studies of evaporation-induced colloidal self-assembly by optical microspectroscopy

Lei Yang, Yiduo Zhang, Jianheng Luo, Yanhong Luo, Kuiyi Gao, Dongmei Li, and Qingbo Meng*
Beijing National Laboratory for Condensed Matter Physics, Institute of Physics, Chinese Academy of Sciences, P. O. Box, 603, Beijing 100190, China
(Received 16 May 2011; revised manuscript received 20 July 2011; published 26 September 2011)

Real-time monitoring of the whole growth process of evaporation-induced colloidal self-assembly has been conducted using an optical microspectroscopy setup. Our observations suggest that the assembly process can be divided into three different growth stages as evidenced by the variations detected in the reflectance spectra. The thickness variation of the growing colloidal crystal was monitored by examining the Fabry-Perot fringes in the reflectance spectra. Furthermore, the scalar wave approximation was utilized to analyze the evolution of optical properties with growth. More detailed information, including the time dependence of number of layers and volume fraction of water, has been revealed by comparing the experimental and calculated reflectance spectra. The present work demonstrates that *in situ* real-time microspectroscopy is a promising technique for monitoring and investigating the dynamic process of colloidal self-assembly.

DOI: 10.1103/PhysRevE.84.031605 PACS number(s): 68.37.−d

I. INTRODUCTION

Three-dimensional photonic crystals, a class of periodically structured materials, provide a new means of tailoring the flow of light and exhibit significant potential for integration of optical devices [1–3]. As typical examples of photonic crystals, colloidal photonic crystals (CPCs) self-assembled from highly monodisperse colloidal spheres have generated a great deal of interest [4–7]. Among all colloidal self-assembly techniques developed to date, evaporation-induced self-assembly (EISA) is probably the most heavily exploited [8–15]. During EISA, spheres are deposited on the substrate placed in an evaporating suspension, and organize spontaneously in an opal structure. The optical properties of the self-assembled CPCs could be easily tuned by controlling the size and material composition of the building blocks. Despite its facility and wider versatility, a critical issue for technological applications is that CPCs fabricated by this approach have inevitable defects. Besides, the current understanding of the microscopic mechanism of the colloidal self-assembly is still limited. Therefore, a thorough understanding and well controlling of the growth of colloidal crystal films by EISA is of great importance from both a fundamental and an applied perspective.

Generally, the growth process in EISA is a dynamic nonequilibrium phenomenon. The real-time observation and *in situ* measurement techniques during growth are therefore very suitable for us to follow the growth dynamics. In the past few years, *in situ* observations of EISA by different types of microscopes have been employed to investigate the mechanism of growth processes from different perspectives, including capillary force [16], water evaporation [17], thickness transitions [18], chemical environment [19], etc. However, in most of the works appearing in the scientific literature, only the growth face parallel to the substrate can be observed directly, whereas it is very difficult to get detailed information about the growth in the third dimension.

In order to obtain the whole three-dimensional growth information, many monitoring techniques, such as x-ray scattering [20], ellipsometry [21], and reflectance spectroscopy [22], have been utilized for real-time studies in growth processes of different kinds of films. As for self-assembly of CPCs, Koh *et al.* utilized reflectance spectroscopy to monitor structure changes during colloidal self-assembly at the meniscus of a sessile drop [23]. Huber *et al.* used energy dispersive x-ray reflectometry to follow *in situ* the dry up of a droplet of colloidal dispersion [24]. Recently, Asher *et al.* monitored the crystal growth kinetics of crystallization of a shear melted crystalline colloidal array by Bragg diffraction fringes [25]. Nevertheless, the whole growth process of CPCs from nucleation to drying in a bulk suspension has not been investigated. The main difficulty of monitoring this widely applied system arises from the low signal to noise ratio and the disadvantage of traditional methods of averaging information over large sample volumes. In such context, we present an experimental investigation of different stages of EISA in a bulk suspension by employing an optical microspectroscopy setup. The elucidation of the growth mechanism is achieved by analyzing a variant of reflectance spectra. Moreover, the time dependence of number of layers and volume fraction of water in the colloidal crystal can be determined by comparing experimental and calculated spectra.

II. EXPERIMENTAL DETAILS

A. Experimental setup

The real-time studies of optical properties of the growing CPCs were performed by employing an optical microspectroscopy setup, which was basically derived from the one used by Ozin *et al.* [26]. As shown in Fig. 1, white light coming from a tungsten bromine lamp (200–2500 nm) was reflected by a beamsplitter, went through a magnification objective×10, and then illuminated the monitored region. The numerical aperture of the objective was 0.25 and its pupil diameter was 9 mm. The aperture diaphragm was adjusted to make the light exactly cover the entrance pupil of the objective. Thus, the size of the monitored region was about 900 μm and it could also be changed by adjusting the aperture diaphragm. Reflected by the sample, the light was collected by the objective and then

*Corresponding author: qbmeng@iphy.ac.cn.

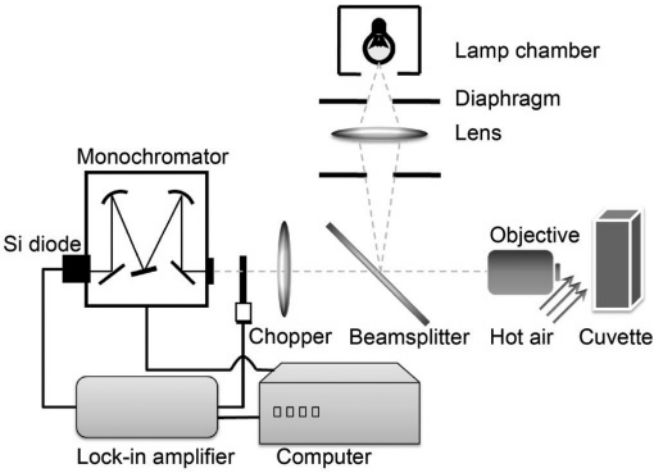

FIG. 1. Schematic diagram of the experimental setup for reflectance measurement.

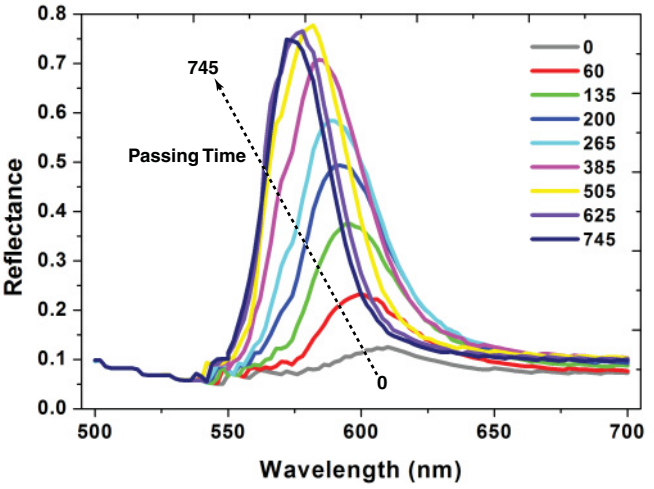

FIG. 2. (Color online) Real time evolution of the reflectivity during EISA at room temperature. The labels indicate the elapsed time in minutes.

went into the monochromator (Omni-λ500, Zolix, Inc., China). After that, the monochromatic light was detected by a Si diode (200–1100 nm) and measured with a lock-in amplifier (SR380, Stanford Research Systems, USA). The chopper placed before the monochromator converted the dc signals into ac signals (180 Hz) to avoid the background noise.

B. Materials and investigated procedure

In our experiment, the CPCs were self-assembled from 2 vol % aqueous suspensions of polystyrene (PS) latex (Duke Scientific Corporation, 240 nm ± 3%) diluted with ultrapure water (Milli-Q Synthesis System, Millipore S.A., Molsheim, France). Just as the *in situ* observation experiment was reported by our group, glass cuvettes were used as the suspension container and their front walls were acting as substrates [17]. Before experiment, these cuvettes were first treated with chromosulfuric acid for more than 3 h, and rinsed copiously with tap water and then with ultrapure water, followed by drying in a stream of nitrogen.

The real-time studies of EISA were carried out under two different conditions: one was at room temperature (25–26 °C); the other was at a relatively high temperature by blowing the front wall of the cuvette with 100 °C hot air (2 cm away from the front wall). After the suspension was placed into the cuvette, which was fixed to a three-dimensional motorized precision stage, it took 24 and 3 h, respectively, for the first measurement to ensure that the process of EISA had become steady. There are few details to be taken care of during experiments: first, the monitored region should be kept in the center of the front wall because the growth process near the edge of the cuvette is considerably altered by the meniscus distortion; and second, at the beginning of the measurement it should be ensured that the whole monitored region is below the top edge of the meniscus so that the whole process of EISA can be monitored. The real-time data acquisition was started as soon as a Bragg diffraction signal from the growing CPC became detectable.

III. RESULTS AND DISCUSSION

A. Different growth stages of EISA monitored at room temperature

First of all, the real time reflectance measurement of EISA at room temperature was carried out. Figure 2 presents a number of reflectance spectra recorded at normal incidence to the substrate. At the very beginning, most of the light is scattered by the homogeneous colloidal suspension. The reflection by growing CPC is so weak that the stop band is not yet evident. We define as zero time for the growth process the instant at which we can detect the weakest Bragg diffraction peak generated by the photonic band gap (PBG) structure nucleating at the cuvette wall. As the growth time proceeds, the stop bands of CPC become more and more distinct and the reflection peak position shifts to shorter wavelength. At later growth stages, the stop-band attenuation is almost constant while the peak position still has certain blue shifts.

Generally, during EISA, colloidal particles are more inclined to self-assemble into a face-centered cubic (fcc) structure which is the most energetically stable for the CPC, and the fcc (111) planes orient parallel to the front wall of the cuvette [17,18]. The diffracted wavelength (λ) from the crystal is given by the Bragg equation [27]

$$m\lambda = 2d_{111}\sqrt{n_{\text{eff}}^2 - \sin^2\theta}, \tag{1}$$

where m is the diffraction order, d_{111} is the interplanar spacing of (111) planes which equals to $(2/3)^{1/2}D$, D is the diameter of colloidal particles, n_{eff} is the effective refractive index of the crystal, and θ is the incident angle. In our case, the incidence angle is zero under normal incidence and the effective refractive index is given by a volume-weighted average:

$$n_{\text{eff}} = \sqrt{0.74n_{\text{PS}}^2 + \psi n_{\text{water}}^2 + (0.26 - \psi)n_{\text{air}}^2}. \tag{2}$$

Here ψ is the volume fraction occupied by water and 0.74 is the volume fraction of spheres for close-packed structure. By

setting $m = 1$, we can get the peak position of the stop band λ_{max}.

The peak position and stop-band attenuation of these reflectance spectra are plotted against the elapsed time to elucidate the different growth stages of EISA [Fig. 3(a)]. According to the optical characteristics of the growing CPC, the whole growing process of EISA in our monitored region could be approximately separated into three stages [Figs. 3(b), 3(c), and 3(d)]. In the first growth stage, corresponding to the first region (T_1) in Fig. 3(a), we monitor the entrance of the growth front into the monitored area and the subsequence rapid CPC growth. As the growth proceeds, the decrease of the peak position goes hand in hand with the increase of the stop-band attenuation. It is well understood that the attenuation monotonically increases with the crystal thickness. Meanwhile, the blue shift of the peak position is due to the increasingly compact lattice. During this period of time, the drying front has not entered the monitored region and the void spaces among the colloids are completely filled with water. As a result, ψ in Eq. (2) equals 0.26 and λ_{max} is calculated to be 598 nm ($n_{eff} = 1.53$) as marked in Fig. 3(a). In the second stage (T_2), the thickness of the CPC continues to increase, the dry front enters the monitored region, and water in the upper region of the growing CPC starts to evaporate. As during the first stage, the attenuation intensity of the diffraction peak increases continuously and the peak position shifts to shorter wavelengths. In the third stage (T_3), the growth front drops out of the monitored region and the thickness of the crystal does not change. The CPC in the monitored region does not grow anymore, but undergoes a drying process. The peak position keeps on shifting to shorter wavelengths with the attenuation remaining at a comparatively high level. In terms of Eq. (1), the blue shifts of the peak position in the second and third stage are mainly caused by the evaporation of water. Theoretically, when the interstices of the CPC in the monitored region are completely out of water, λ_{max} should be 571 nm ($\psi = 0$, $n_{eff} = 1.46$), which is a little lower than the data points we have obtained [Fig. 3(a), region (T_3)]. The specific variation of the volume fraction of water in the crystal due to the evaporation will be discussed later. Additionally, it is notable that the attenuation has a little degradation when the drying stage comes to the end. It is believed that the observed reduction in reflectance should mainly originate from defects and cracks caused by the drying process.

The time dependence of the CPC thickness can also be extracted from the measured real-time reflectance spectra. Here the thickness of the crystal is estimated by Fabry-Perot (FP) fringe analysis derived by Colvin *et al.* [8], namely,

$$T = \frac{p\lambda_1\lambda_p}{2n_{eff}(\lambda_1 - \lambda_p)}, \tag{3}$$

where T is the film thickness, p is a positive integer numbering consecutive maxima from the long-wavelength fringe p_1, and λ_1/λ_p are the wavelength corresponding to fringe orders p_1/p, respectively. In the initial stage of growth, the growing film has covered only a small area of the monitored region and the polydispersity in film thickness is comparatively high [as illustrated in Fig. 3(b)]. Thus, the reflectance spectra at growth times smaller than 200 min do not exhibit well-regulated FP fringes. As the growth proceeds, a film of lower

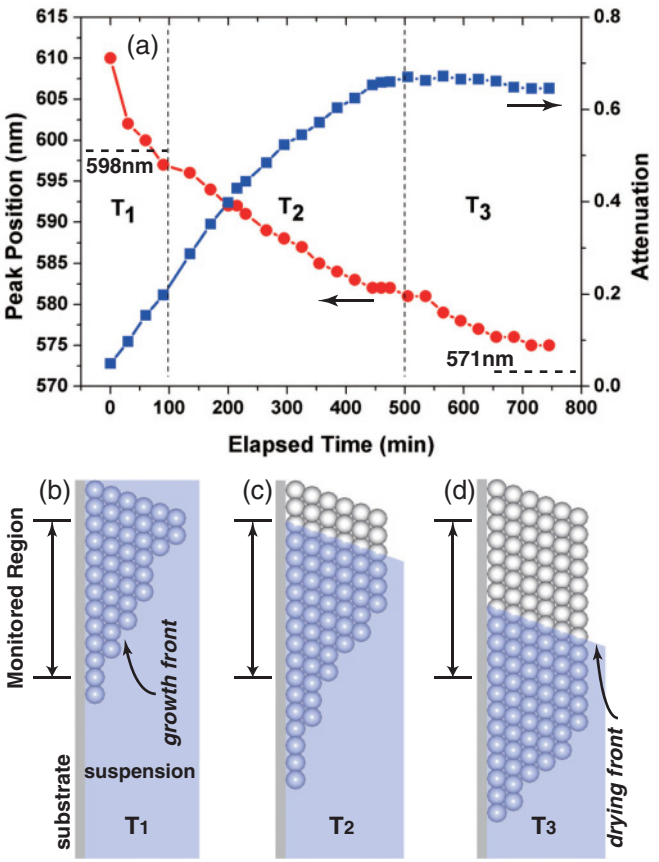

FIG. 3. (Color online) (a) The peak position (red circles) and stop-band attenuation (blue squares) as functions of the elapsed time. These data points are obtained from the reflectance spectra recorded in the real-time monitoring experiment at room temperature (partially shown in Fig. 2). Schematic diagram for the EISA growth process of different stages: (b) only the growth front, (c) both the growth front and the drying front, and (d) only the drying front, under the monitored region.

thickness polydispersity gradually covers a large part of the monitored region, and higher contrast FP fringes begin to appear [as shown in Figs. 4(a) and 4(b)]. The film thickness is calculated by using fringes pairs furthest away from the Bragg diffraction peak. Although the relative intensity of these FP fringes compared with the attenuation of the Bragg diffraction peak is rather small, the position of the fringes can be easily determined and yield precise values for CPC film thickness. As already mentioned, the parameter n_{eff} is varying from 1.53 to 1.46 during the CPC growing and drying processes. The red circles in Fig. 4(c) are calculated by setting $n_{eff} = 1.46$ (interstices filled entirely with air) while the blue squares by setting $n_{eff} = 1.53$ (interstices filled entirely with water). In fact, the actual thickness variations with the elapsed time should be some curve between the red circles and blue squares. Furthermore, this actual curve should get closer and closer to, and finally coincide with the red circles because of the water evaporation. Since the effective refractive index in Eq. (3) is varying during growth, the FP analysis here is not aimed at calculating the film thickness extremely accurately. Analysis of reflectance spectra by the scalar wave approximation (discussed later) would take this

factor into account. Nevertheless, both the time dependence of CPC thickness and properties of Bragg diffraction peak correspond well with each other [see Figs. 3(a) and 4(c)], which further confirms the three-stage growth mechanism. In order to further validate our analysis, the final thickness of CPC is characterized by a profilometer (Product P-6, KLA Tencor Corporation, USA). Figure 5(a) presents the heights of CPC along the vertical direction relative to the substrate. From right to left (growth direction), the film starts to grow thick at the beginning and then undergoes distinct thickness fluctuations over a long distance. Thicknesses of CPC along the horizontal position at 6.52 and 8.77 mm are measured and shown in Fig. 5(b). As we mentioned above, because of the influence of the cuvette corner, the film is much thicker on both sides of the front wall. Basically, our monitored region is around the central axis (3–4 mm along the horizontal position, 7–8 mm along the vertical position), where the thickness is comparatively uniform. The average thickness from 6.52 to 8.77 mm along the central axis in the vertical direction is measured to be 13.56 μm, which is comparable with the final thickness of 13.95 μm calculated by FP fringe analysis.

B. Analysis of reflectance spectra by the scalar wave approximation (SWA)

Since the growth rate of CPCs at room temperature is very slow, we introduced a controlled hot air stream to accelerate the growth process. Therefore, the reflectance spectra are more sensitive to the elapsed time, and the number of layers variations in a very short time have been analyzed by a tractable model based on SWA. It is very appropriate for this simple model to calculate analytical expressions for the reflectance and transmittance of CPCs when electromagnetic propagation along only one particular direction of the crystal (e.g., the [111] axis) is taken into account [28,29]. Although full details on SWA have been discussed in the literatures [30–32], some additional assumptions in our case should be made when applying this method. First, the growth process of EISA is not a simple layer-by-layer growth. Different layers have different coverage areas of colloidal spheres. Thus, the entire analysis should rely on the assumption that the growing film has a homogeneous thickness. Second, no matter which stage ($T_1/T_2/T_3$) the growth process goes through, the medium after transmission is always supposed to be air. We are concerned solely with the reflectance of the growing crystal. Last, the filling fraction of PS spheres is a constant. In the present work, it should be noted that the film under consideration is grown on the front wall of the cuvette. The incident light first goes through the substrate and then the crystal, which is opposite to the normal condition. So, in terms of all these considerations, reflectance is determined by the following analytical expression:

$$R = \left| \frac{(1+\beta)(1+\eta)k_i - (1-\beta)[k_c + \eta(k_c - G)]}{(1+\beta)(1+\eta)k_i + (1-\beta)[k_c + \eta(k_c - G)]} \right|^2, \quad (4)$$

where

$$\beta = \frac{(k_c - k_t)e^{ik_cT} + \eta(k_c - k_t - G)e^{i(k_c-G)T}}{(k_c + k_t)e^{-ik_cT} + \eta(k_c + k_t - G)e^{-i(k_c-G)T}}. \quad (5)$$

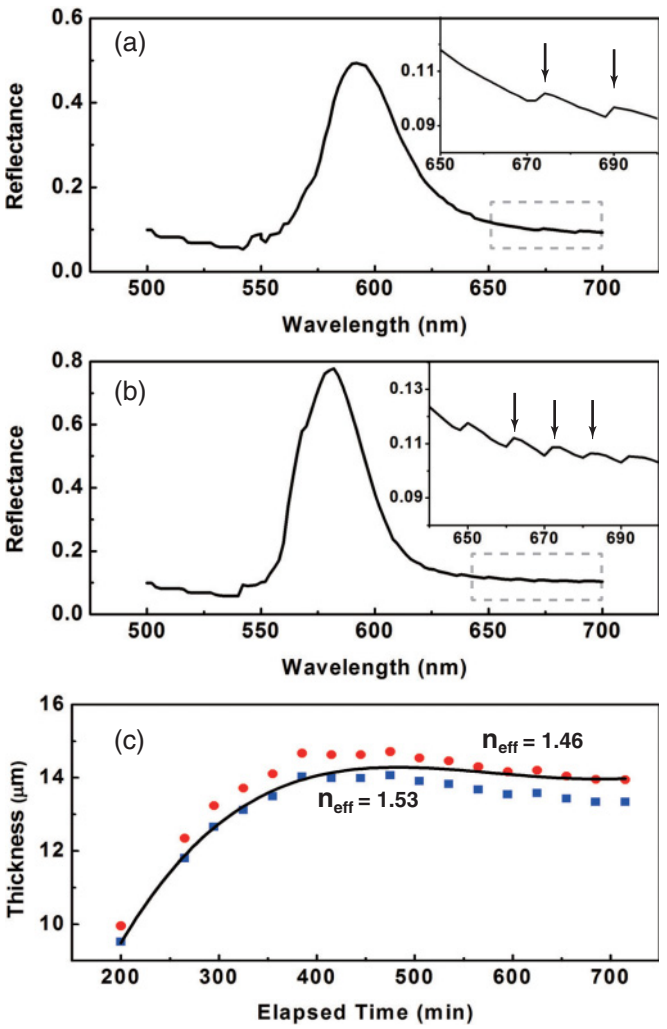

FIG. 4. (Color online) Normal incidence reflectance spectra recorded at the elapsed time of: (a) 200 min and (b) 505 min. The insets, which are obtained from magnifying the rectangle regions, show the closely spaced Fabry-Perot fringes. (c) Calculated thickness of the growing CPC as a function of the elapsed time by using Eq. (3) with $n_{\text{eff}} = 1.46$ (red circles) and $n_{\text{eff}} = 1.53$ (blue squares). The polynomial fitting curve indicates the actual thickness variations.

Here, k_i and k_t are the wave vectors in the homogeneous incident (glass) and outgoing (air) media, respectively, k_c is the wave vector inside the photonic crystals, T is the thickness of the photonic crystals, G is the magnitude of the reciprocal lattice vector, and η is the dielectric contrast between the two materials which comprise the composite structure. The analytical expressions of these parameters and the dispersion relation are defined in detail in Ref. [31].

For the sake of comparison, both experimental reflectance spectra at different times and simulative results using the SWA are shown together in Fig. 6. The reflectance spectra are calculated by considering the filling fraction of spheres $f_{\text{sphere}} = 0.74$, the particle and water refractive index of $n_{\text{PS}} = 1.59$ and $n_{\text{water}} = 1.33$, respectively. Thus, the analytical expression for the reflectance of the crystal is a function of the sphere size, the effective refractive index of the crystal, and number of layers (N) in the [111] direction of the fcc

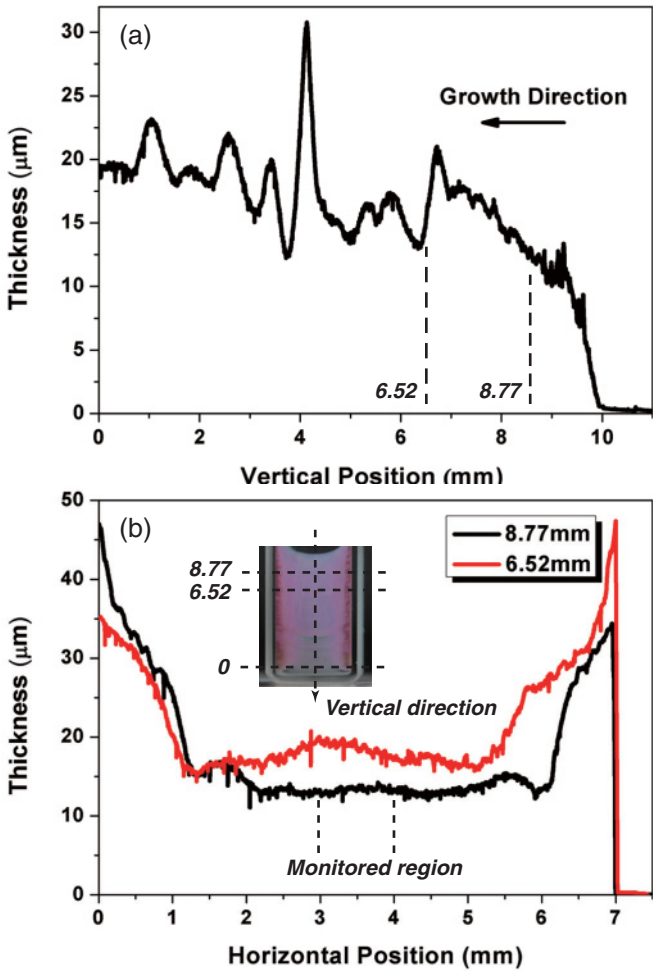

FIG. 5. (Color online) The post-growth heights of CPC relative to the substrate measured by a profilometer: (a) along the central axis and (b) along the horizontal direction at 8.77 and 6.52 mm, respectively. The inset shows the photograph of a post-growth film deposited on the front wall of the cuvette.

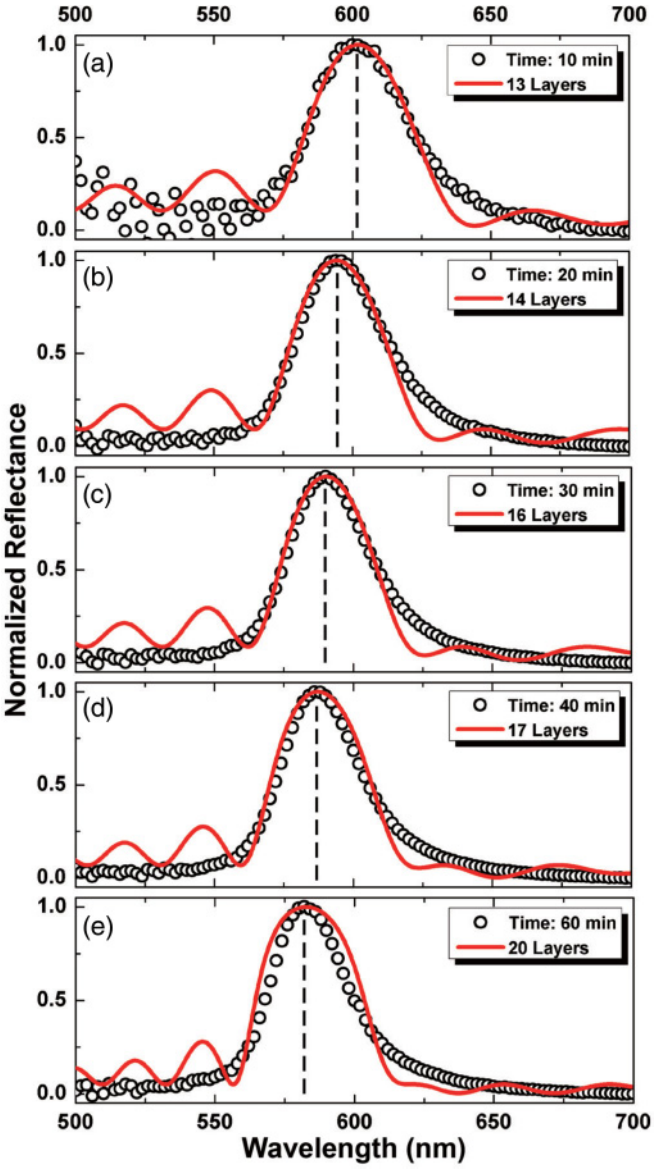

FIG. 6. (Color online) Normal-incidence reflectance spectra for the growing CPC under a hot air stream at different times (circles). The red solid curves are calculated using the SWA with parameters: (a) $D = 246$ nm, $n_{\text{eff}} = 1.53$; (b) $D = 242$ nm, $n_{\text{eff}} = 1.53$; (c) $D = 240$ nm, $n_{\text{eff}} = 1.53$; (d) $D = 240$ nm, $n_{\text{eff}} = 1.52$; and (e) $D = 240$ nm, $n_{\text{eff}} = 1.49$. The dashed lines highlight the peak position variations.

structure. Above all, the reflectance spectrum at the critical time separating stage one and stage two is simulated by fixing the parameters $D = 240$ nm, $n_{\text{eff}} = 1.53$ ($\psi = 0.26$), and changing number of layers. It is found that only when the elapsed time is at 30 min, both the peak position and full-with at half-maximum (FWHM) of the simulations agree well with the experimental data, as shown in Fig. 6(c). Before this critical time, the drying front is out of the monitored region, so the effective refractive index is 1.53 constantly. The blue shift of peak position is caused by the lattice parameter variations and the equivalent sphere size is simulated to be 246 nm at 10 min and 242 nm at 20 min, respectively. After the critical time, we assume that the lattice parameter is fixed at 240 nm. It is the evaporation of water in the crystal that makes the peak position move to the shorter wavelength. The effective refractive index is simulated to be 1.52 at 40 min and 1.49 at 60 min, respectively. However, what needs to be stressed is that the critical time is not so clear cut. Both lattice parameter variations and evaporation of water can give rise to the blue shift of peak position in stage two (T_2). And it is simply the effective refractive index that plays the dominant role. Besides, it is worth noting that the experimental spectra shown in Fig. 6 do not exhibit FP fringes. In terms of the complicated dynamic process of EISA, many factors influence the optical properties of the growing film, including the degree of order in the CPC, film thickness, medium in the interstices of the crystal, and so on. The combined effect of all these factors determines the observed loss of visibility of the FP fringes.

Figure 7(a) displays the peak position and stop-band attenuation of the reflectance spectra to entirely illustrate the whole growth process with a hot air stream. It is found that the variations of optical properties under different growth conditions exhibit similar trends. The differences between the two conditions are that the peak position and the attenuation change more quickly due to the faster evaporation and growth

rate of CPC with the hot air stream. Moreover, according to the study of Colvin *et al.*, the broad stop-band bandwidth is a fundamental property of close-packed spherical arrays [28]. In terms of the result of SWA, the bandwidth exhibits a more dramatic change in behavior at the critical thickness than the peak attenuation. The critical thickness N_c of close-packed spheres is given by

$$N_c = \frac{1}{\pi}\left[\sqrt{4+\left(\frac{K\psi_0}{\psi_0+1}\right)^2}-2\right]^{-1/2}, \tag{6}$$

where $K = (2/\alpha^3)(\sin\alpha - \alpha\cos\alpha)$, and where $\alpha = 2\pi\sqrt{3/8}$. For the close-packed PS-water films in our case, $N_c = 20$ layers, and for the PS-air films, $N_c = 9$ layers. The inset in Fig. 7(b) indicates that the stop-band bandwidth for a colloidal crystal of a given thickness is a sensitive function of dielectric contrast ψ_0. Considering that the dielectric contrast is varying during the evaporation process of EISA, it is very suitable here for us to characterize the optical properties with FWHM. Figure 7(b) shows the stop-band bandwidths as a function of elapsed time, indicating that the variations of FWHM are consistent with the separation of the growing process into three different stages. The bandwidth narrows rapidly due to the growing thickness of the CPC in stage one and two (0–70 min). Moderate drying process improves the crystallinity of the CPC while excessive drying introduces unavoidable defects and cracks, thus the bandwidth shows the tendency to decrease first and increase later in the stage of drying (70–400 min). Besides, number of layers and volume fraction of water in the crystal at different times were obtained by fitting the reflectance spectra with SWA [Figs. 7(b) and 7(c)].The number of layers becomes a constant from time ~70 min onwards while the bandwidth still has certain variations. The analysis is based on the conclusion that the film thickness stops growing at the elapsed time of 70 min. This conclusion was reached as a consequence of two observations: first, as shown in Fig. 7(a), the attenuation stops increasing from time ~70 min onwards. Given that the thickness of the film still grows, the attenuation of the Bragg diffraction peak would definitely increase. Second, during this real-time monitoring experiment, it is evident that the growth front is far from the bottom edge of the monitored region when the elapsed time is above ~70 min.

Finally, we consider a very simple evaporation model. By assuming that the growth rate of the film equals the evaporation rate of water, the distance between the growth and dry front can be considered to be a constant l_0. Therefore, the volume fraction of water f_{water} can be simply written as

$$f_{\text{water}} = \begin{cases} 0.26 & (t \leqslant t_1) \\ 0.26 l_0/[V_e(t-t_1)+l_0] & (t_1 \leqslant t \leqslant t_2) \\ 0.26[l_0 - V_e(t-t_2)]/L & (t \geqslant t_2), \end{cases} \tag{7}$$

where V_e is the evaporation rate of water, t_1 and t_2 are the characteristic times separating the three growth stages, and L is the size of the post-growth photonic crystal in the monitored region. The curve fitted by Eq. (7) is plotted in Fig. 7(c), and the fitted distance between the growth and dry front is about 350 μm. It is found that the volume fraction of water extracted from the SWA is in good agreement with this simple evaporation model.

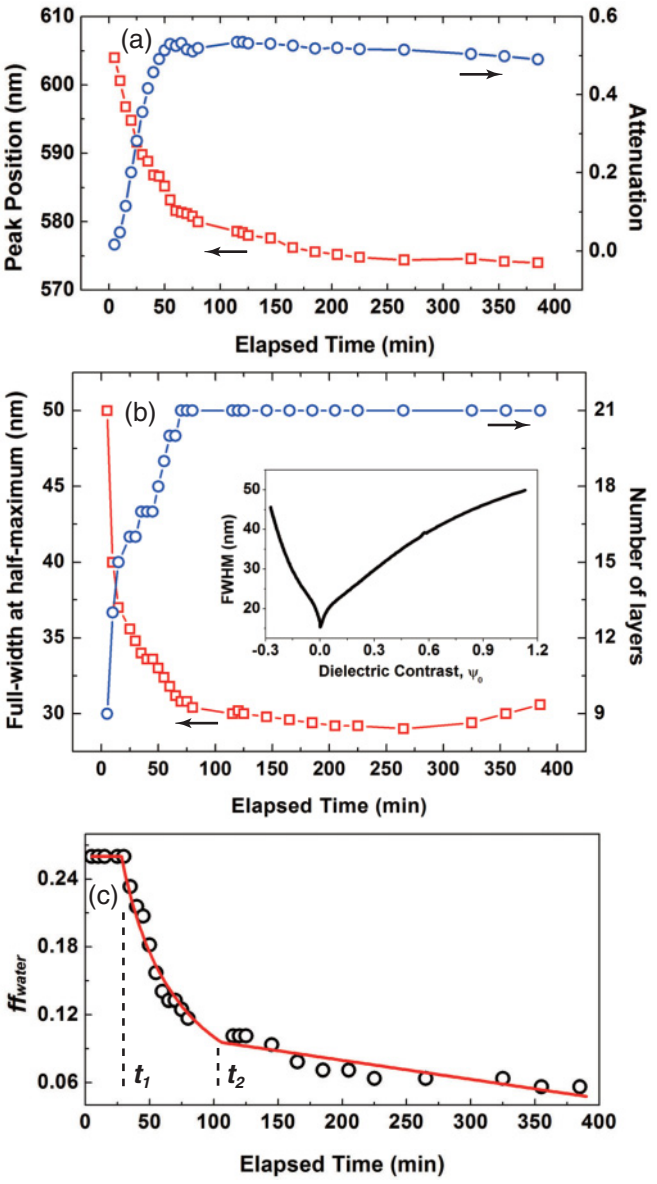

FIG. 7. (Color online) Real-time studies of the faster growth process of EISA introduced by a hot air stream. (a) The peak position (red squares) and stop-band attenuation (blue circles) vs elapsed time. (b) Experimental full-with at half-maximum and calculated number of layers as functions of the elapsed time. The inset shows the stop-band width for a single 20-layer colloidal crystal of 240 nm PS spheres, as a function of dielectric contrast ψ_0, calculated by the SWA. (c) Volume fraction of water in the crystal as a function of the elapsed time. The open circles are extracted from the SWA, while the red solid curve represents the best fit obtained using Eq. (7).

IV. CONCLUSIONS

Real-time studies of the entire growth process of CPC films by EISA have been realized by an optical microspectroscopy setup. The evolution of optical properties, including the peak position, stop-band attenuation, and FWHM, indicates that the growth process of CPC under the monitored region can be separated into three stages. The thickness of the growing CPC as a function of the elapsed time was estimated by

Fabry-Perot fringe analysis. In addition, the acceleration of the EISA process by a hot air stream was monitored *in situ*. Comparison between experimental and calculated reflectance spectra enable us to extract the time dependence of number of layers and volume fraction of water in the photonic crystal. The detailed information obtained provides a deep insight into both the growth and drying process. This work demonstrates that real-time reflectance measurement is a powerful approach to understanding the direct relation between structural and optical properties of CPCs during self-assembly. Future work will address additional kinetic aspects of CPC nucleation and growth by EISA.

ACKNOWLEDGMENTS

The authors appreciate the financial support from the Natural Science Foundation of China (No. 20725311, No. 20873178, and No. 51072221) and Foundation of the Chinese Academy of Sciences (No. KJCX2-YW-W27).

[1] E. Yablonovitch, Phys. Rev. Lett. **58**, 2059 (1987).
[2] S. John, Phys. Rev. Lett. **58**, 2486 (1987).
[3] J. D. Joannopoulos, P. R. Villeneuve, and S. H. Fan, Nature (London) **386**, 143 (1997).
[4] R. Rengarajan, P. Jiang, D. C. Larrabee, V. L. Colvin, and D. M. Mittleman, Phys. Rev. B **64**, 205103 (2001).
[5] A. Arsenault, S. B. Fournier-Bidoz, B. Hatton, H. Miguez, N. Tetrault, E. Vekris, S. Wong, S. M. Yang, V. Kitaev, and G. A. Ozin, J. Mater. Chem. **14**, 781 (2004).
[6] N. Tetreault, A. Mihi, H. Miguez, I. Rodriguez, G. A. Ozin, F. Meseguer, and V. Kitaev, Adv. Mater. **16**, 346 (2004).
[7] E. Vekris, V. Kitaev, D. D. Perovic, J. S. Aitchison, and G. A. Ozin, Adv. Mater. **20**, 1110 (2008).
[8] P. Jiang, J. F. Bertone, K. S. Hwang, and V. L. Colvin, Chem. Mater. **11**, 2132 (1999).
[9] Q. B. Meng, Z. Z. Gu, O. Sato, and A. Fujishima, Appl. Phys. Lett. **77**, 4313 (2000).
[10] Y. H. Ye, F. LeBlanc, A. Hache, and V. V. Truong, Appl. Phys. Lett. **78**, 52 (2001).
[11] Z. Z. Gu, A. Fujishima, and O. Sato, Chem. Mater. **14**, 760 (2002).
[12] S. Wong, V. Kitaev, and G. A. Ozin, J. Am. Chem. Soc. **125**, 15589 (2003).
[13] S. H. Im, M. H. Kim, and O. O. Park, Chem. Mater. **15**, 1797 (2003).
[14] Z. Y. Zheng, X. Z. Liu, Y. H. Luo, B. Y. Cheng, D. Z. Zhang, Q. B. Meng, and Y. R. Wang, Appl. Phys. Lett. **90**, 051910 (2007).
[15] Z. Y. Zheng, K. Y. Gao, Y. H. Luo, D. M. Li, Q. B. Meng, Y. R. Wang, and D. Z. Zhangt, J. Am. Chem. Soc. **130**, 9785 (2008).
[16] A. S. Dimitrov and K. Nagayama, Langmuir **12**, 1303 (1996).
[17] L. Yang, K. Y. Gao, Y. H. Luo, J. H. Luo, D. M. Li, and Q. B. Meng, Langmuir **27**, 1700 (2011).
[18] L. L. Meng, H. Wei, A. Nagel, B. J. Wiley, L. E. Scriven, and D. J. Norris, Nano Lett. **6**, 2249 (2006).
[19] Q. Yan, L. Gao, V. Sharma, Y. M. Chiang, and C. C. Wong, Langmuir **24**, 11518 (2008).
[20] E. Weschke, C. Schussler-Langeheine, R. Meier, G. Kaindl, C. Sutter, D. Abernathy, and G. Grubel, Phys. Rev. Lett. **79**, 3954 (1997).
[21] V. Burtman, Y. Ofir, and S. Yitzchaik, Langmuir **17**, 2137 (2001).
[22] T. Okubo and H. Ishiki, J. Colloid Interface Sci. **228**, 151 (2000).
[23] Y. K. Koh and C. C. Wong, Langmuir **22**, 897 (2006).
[24] P. Huber, T. Blattler, M. Textor, W. Leitenberger, U. Pietsch, and T. Geue, Colloids Surf. A **321**, 113 (2008).
[25] J. J. Bohn, A. Tikhonov, and S. A. Asher, J. Colloid Interface Sci. **350**, 381 (2010).
[26] H. Miguez, S. M. Yang, and G. A. Ozin, Appl. Phys. Lett. **81**, 2493 (2002).
[27] C. Lopez, L. Vazquez, F. Meseguer, R. Mayoral, M. Ocana, and H. Miguez, Superlattices Microstruct. **22**, 399 (1997).
[28] J. F. Bertone, P. Jiang, K. S. Hwang, D. M. Mittleman, and V. L. Colvin, Phys. Rev. Lett. **83**, 300 (1999).
[29] G. von Freymann, S. John, S. Wong, V. Kitaev, and G. A. Ozin, Appl. Phys. Lett. **86**, 053108 (2005).
[30] S. Satpathy, Z. Zhang, and M. R. Salehpour, Phys. Rev. Lett. **64**, 1239 (1990).
[31] D. M. Mittleman, J. F. Bertone, P. Jiang, K. S. Hwang, and V. L. Colvin, J. Chem. Phys. **111**, 345 (1999).
[32] K. W. K. Shung and Y. C. Tsai, Phys. Rev. B **48**, 11265 (1993).